ISSN 0020-1685, Inorganic Materials, 2019, Vol. 55, No. 12, pp. 1290–1296. © Pleiades Publishing, Ltd., 2019.
Russian Text © The Author(s), 2019, published in Neorganicheskie Materialy, 2019, Vol. 55, No. 12, pp. 1368–1374.

Porous Reaction-Bonded Silicon Nitride Ceramics: Fabrication Using Hollow Polymer Microspheres and Properties

N. K. Georgiu[a], *, I. F. Georgiu[a], K. V. Klemazov[a], M. G. Lisachenko[a], A. O. Zabezhailov[a], and M. Yu. Rusin[a]

[a]*JSC Romashin Tekhnologiya Research and Production Enterprise, Kievskoe sh. 15, Obninsk, Kaluga oblast, 249030 Russia*
**e-mail: nkceram@gmail.com*

Received November 21, 2018; revised June 10, 2019; accepted July 3, 2019

Abstract—A process has been proposed for the preparation of porous reaction-bonded silicon nitride (RBSN) via the addition of a pore former, uniaxial pressing, and subsequent reaction sintering in a vacuum furnace. As a pore former, we used a commercially available powder consisting of hollow polymer microspheres (Akzonobel) with an average diameter of 9 μm. We have studied the effect of pore former content in green compacts on the mechanical, dielectric, and thermophysical properties of the ceramics. The proposed process allows one to prepare porous RBSN with the following properties: σ_b = 48 MPa, ε = 3.2, tan δ = 35×10^{-4} at a frequency of 10 GHz, and λ = 0.96 W/(m K) at 1100°C. The ceramic obtained in this study is potentially attractive for industrial application as a radar-transparent structural material with reduced thermal conductivity.

Keywords: reaction-bonded silicon nitride, porous ceramics, structural ceramics, pore former
DOI: 10.1134/S0020168519120057

INTRODUCTION

Reaction-bonded silicon nitride (RBSN) ceramics are among the few materials offering a combination of properties required for the fabrication of heat-loaded elements of structures for aerospace applications. In particular, RBSN possesses high mechanical strength (σ_b = 200–300 MPa), thermal stability (long-term stability at 1400°C and short-term stability up to 1900°C), and rain and dust erosion resistance, and retains its dielectric characteristics in a wide temperature range [1–3].

At the same time, the relatively high thermal conductivity of silicon nitride ceramics (~20 W/(m K) at 20°C) can limit potential applications of the material. In particular, this poses the problem of protecting radioelectronic systems from overheating during flight of high-speed aircraft [4].

The thermal conductivity of Si_3N_4 ceramics depends on many factors, such as porosity, the pore size distribution, lattice defects, morphology of crystals, impurities, relative amounts of the α- and β-polymorphs, and others [5–8]. According to theoretical calculations, the thermal conductivity of α- and β-Si_3N_4 single crystals is approximately 105 and 225 W/(m K) along the crystallographic axis *a* and 170 and 450 W/(m K) in the *c*-axis direction, respectively [9]. Commercially available RBSN-based Si_3N_4 ceramic materials typically have a polycrystalline structure and considerably lower thermal conductivity, from 10 to 30 W/(m K).

There were attempts to produce silicon nitride-based materials with reduced thermal conductivity (~0.5–3 W/(m K)) by increasing its porosity to 40–60% [10, 11]. High-porosity silicon nitride can be produced by a number of well-known techniques, for example, by utilizing a pore former [12, 13], freeze drying [14], foaming [15–17], gel casting [18], flash combustion [19], etc.

The addition of a pore former allows one to produce porous ceramics with porosities from 40 to 60%. This method has the drawback that the pore distribution over the material is nonuniform because of the inhomogeneous pore former distribution in the mixing and molding steps. Foaming makes it possible to produce low-density open-cell ceramic foams with porosities in the range 75–90%, which are used primarily as refractories and filtering materials. This approach has a number of drawbacks: relatively large pore size (100–400 μm), small pore wall thickness, and, as a consequence, low strength (1–5 MPa). Other methods are less widespread because they are technologically difficult to implement, require expensive apparatus, or have a narrow application area.

In addition to the limitation related to its thermal conductivity, the use of RBSN can be impeded by the fact that its dielectric permittivity (ε ~ 5.6–6.3 at a frequency of 10 GHz) is rather high for radar-transparent

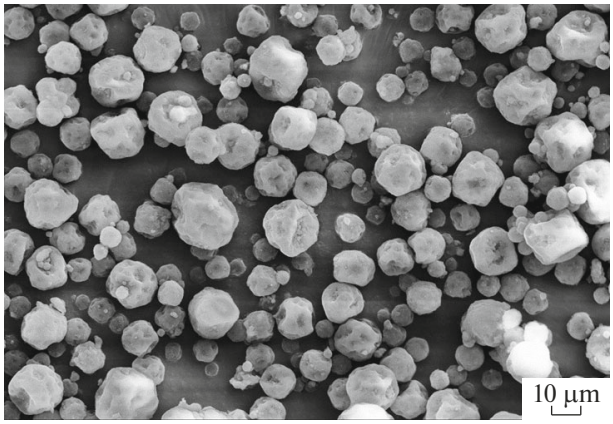

Fig. 1. SEM micrograph of the pore former.

components [4, 20]. The dielectric permittivity of ceramic materials is known to decrease with increasing porosity, but this is accompanied by strength loss. The strength of porous ceramics depends on not only the density and strength of their solid component [21] but also the porosity and pore size [22, 23]. Moreover, the largest contribution to strength loss is made by large pores, more than 20 μm in diameter, which act as stress risers [22, 23]. Thus, processes for the preparation of porous RBSN that allow one to control the pore size in the material are of practical interest.

One example of the preparation of porous silicon nitride with controlled pore size was reported by Zhou et al. [24]. They proposed a process for the preparation of highly porous sintered silicon nitride and examined the effect of the size and amount of a pore former on the strength and dielectric properties of the ceramic.

Park et al. [25] proposed a process for the preparation of RBSN with porosity in the range 48–52% and assessed the effect of pore size on the strength of the material.

In the studies mentioned above, no thermophysical properties of the materials were investigated.

In this paper, we report the preparation of highly porous RBSN by a method that combines the addition of a pore former (filler) and uniaxial pressing, followed by reaction sintering.

EXPERIMENTAL

Semiconductor-grade silicon was ball-milled for 24 h to give Si powder with $d_{50} \sim 8$ μm. As a pore former, we used commercially available methylmethacrylate/acrylonitrile copolymer microspheres (Akzonobel) with an average particle diameter of 9 μm (Fig. 1).

The process for the preparation of highly porous RBSN is schematized in Fig. 2. The main steps are the preparation of preceramic powder, compaction, removal of the pore former, and subsequent reaction sintering.

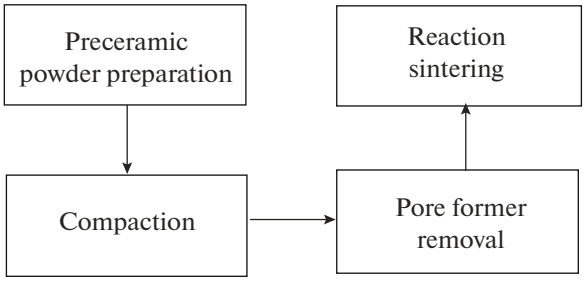

Fig. 2. Block diagram of the porous RBSN preparation process.

Preceramic powder was prepared as follows: To an aqueous 3% polyvinyl alcohol solution were sequentially added polymer microspheres, an ammonium polyacrylate-based surfactant (Dolapix CE 64), and silicon powder. We used (silicon + pore former) compositions containing 5, 10, 15, 25, 30, and 40 wt % pore former. To these compositions was added the surfactant (0.5 wt %). The components were mixed using a high-speed mixer. The resultant suspension was dried to a humidity from 18 to 20% and then sequentially rubbed through a 800- and a 400-μm steel sieve in a rubbing machine. The powder thus prepared was dried further to a humidity from 6 to 8% and then pressed into beams and disks at 100, 150, and 200 MPa on a uniaxial press.

In the next step, the green compacts were placed into a muffle furnace to remove the pore former. The firing schedule was chosen using simultaneous thermal analysis (STA) data obtained for the pure pore former in flowing air at a heating rate of 10°C/min (Fig. 3).

Since pore former decomposition was an exothermic reaction, the compacts were thermostated at the temperatures corresponding to the most active heat release to avoid their disintegration as a result of vigorous gas evolution. The samples were placed on silicon nitride substrates and heated to 620°C over a period of 24 h and then furnace-cooled. After the removal of the pore former, the compacts were loaded into a vacuum furnace and nitrided while the temperature was raised to 1450°C.

The resultant ceramics were machined to produce beams 7 × 7 × 60 or 4 × 4 × 50 mm in dimensions and disks 49.5 mm in diameter and 4.5 mm in thickness. The apparent density ρ and open porosity Π_o were determined by hydrostatic weighing in water at room temperature. First, the ceramic samples were held at 170°C for 2 h and degassed in vacuum for 20 min. The samples were filled with water under vacuum. The bending strength σ_b was determined in three-point bend tests in conformity with the Russian Federation State Standard GOST 24409-80, using a support span of 50 mm and a crosshead speed of 1.5 mm/min. The dielectric permittivity ε and dielectric loss tangent tan δ

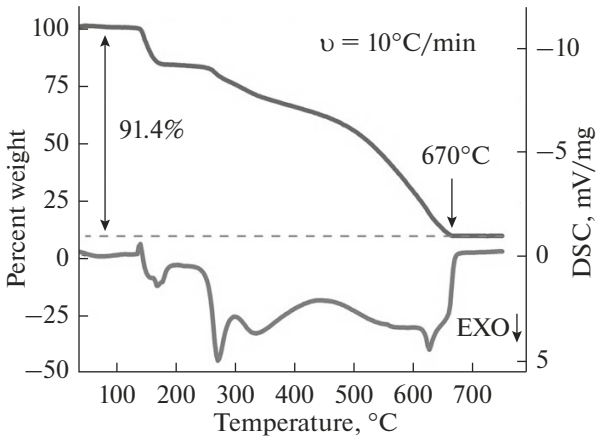

Fig. 3. STA curve of the pore former.

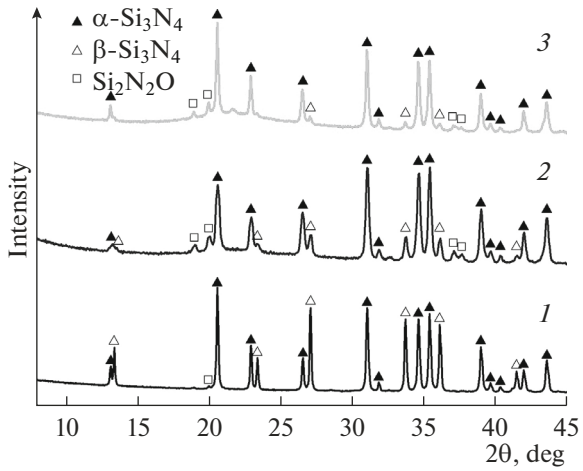

Fig. 4. X-ray diffraction patterns of the porous RBSN samples prepared using preceramic powders containing (*1*) 10, (*2*) 30, and (*3*) 40% pore former.

were determined at a frequency of 10 GHz and a temperature of 20°C.

The phase composition of the ceramics was determined by X-ray diffraction on a DRON-6 diffractometer (CuK_α radiation). The microstructure of the ceramics was examined by scanning electron microscopy (SEM) on an EVO 40XVP. The pore size distribution was determined by Hg porosimetry using a Pascal 140/440 instrument.

The linear thermal expansion coefficient (LTEC) was determined in air in the range 20 to 900°C with a Netzsch DIL 402C dilatometer in conformity with the Russian Federation State Standard GOST 10978-2014. The thermal diffusivity a of specimens 10 × 10 × 2.5 mm in dimensions was determined in air at temperatures of up to 700/1100°C by the laser flash method using a Netzsch LFA 457 system. Heat capacity C_p was determined by differential scanning calorimetry (DSC) in the temperature range from 20 to 1100°C in flowing nitrogen using a Netzsch DSC 404F1 instrument. Thermal conductivity λ was calculated from the measured density, heat capacity, and thermal diffusivity.

RESULTS AND DISCUSSION

The X-ray diffraction data in Fig. 4 demonstrate that the porous ceramic obtained consisted of α- and β-Si_3N_4 and a small amount of Si_2N_2O.

Comparison of the intensity of reflections from α- and β-Si_3N_4 in samples *1–3* shows that increasing the pore former content of the preceramic powder increases the percentage of the α-phase in the ceramic (Table 1). The α-Si_3N_4 content of the ceramic prepared using the powder containing 40% pore former was 75%, suggesting that the nitridation reaction went to near completion before the silicon began to melt (1410°C). This is expected to allow for a reduction in the maximum reaction sintering temperature in the preparation of porous RBSN.

Table 2 illustrates the influence of pore former content and compaction pressure on the strength and dielectric properties of the ceramics.

There is a tendency for the apparent density and bending strength to decrease with increasing pore former content, which is accompanied by an increase in porosity. The data in Table 2 were used to plot the bending strength against open porosity (Fig. 5).

The observed behavior is well consistent with previously reported data [26]. At the same time, the σ_b of the ceramic samples obtained after pressing at 200 MPa exceeds previously reported values for RBSN ceramics with 50% porosity. For example, Park et al. [25] reported that the strength of RBSN samples with porosities in the range 48–54% did not exceed 31 MPa. They attributed it to the presence of large pores, ~100 μm in diameter, in the material.

To assess the effect of compaction pressure on the strength of the ceramics, we plotted their bending strength against pore former content at different compaction pressures (Fig. 6).

It is seen that there is a clear correlation between the strength of the ceramics and compaction pressure.

Table 1. Major crystalline phases in the porous RBSN ceramics

Percent of the pore former	Phase composition, %		
	α-Si_3N_4	β-Si_3N_4	Si_2N_2O
10	55	34	5
30	68	15	9
40	75	6	11

Table 2. Influence of pore former content and compaction pressure on the properties of porous RBSN

Weight percent of the pore former in the compacts	Compaction pressure, MPa	ρ, g/cm^3	Π_o, %	σ, MPa	ε ($f = 10^{10}$ Hz)	$\tan\delta \times 10^4$
5	100	2.4	26	134	5.5	23
	150	2.4	24	155		
	200	2.5	22	166		
10	100	2.2	29	109	5.3	26
	150	2.3	29	131		
	200	2.4	28	158		
15	100	2.1	35	100	4.7	24
	150	2.2	33	111		
	200	2.2	30	124		
25	100	1.8	44	75	3.9	24
	150	1.9	41	82		
	200	1.9	40	81		
30	100	1.7	47	55	3.6	29
	150	1.8	45	66		
	200	1.8	44	77		
40	100	1.5	53	39	3.2	35
	150	1.5	52	42		
	200	1.6	50	48		

The bending strength of the porous RBSN produced via compaction at 200 MPa is on average 10% higher than that of the ceramic produced via compaction at 150 MPa and 20% higher than that of the ceramic produced via compaction at 100 MPa.

The observed increase in the strength of the porous ceramics is due to the densification of the solid component of the material. At 200 MPa, we observe no strength saturation; that is, further densification of the compacts is possible. Therefore, it is reasonable to expect that higher strength of porous ceramics can be reached at higher compaction pressures.

Since the strength of the ceramics depends on not only total porosity but also the pore size, we performed porosity measurements with a mercury porosimeter. The results were used to obtain the pore size distribution for the porous RBSN samples with $\Pi_o = 52$ and 17% (Fig. 7).

The samples have the same average pore size, but the highly porous silicon nitride has a broader pore

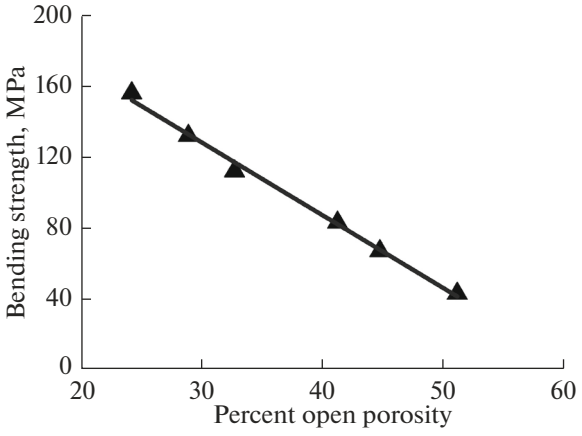

Fig. 5. Bending strength as a function of open porosity.

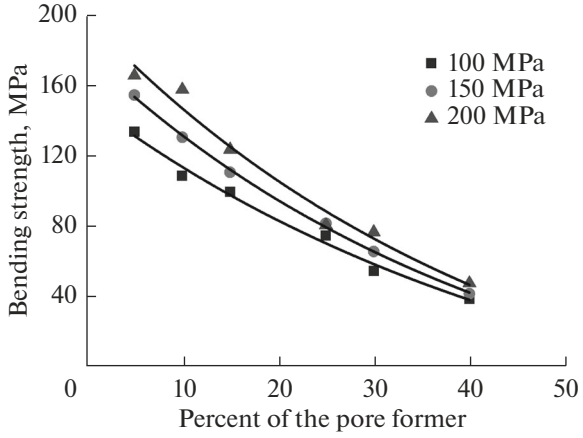

Fig. 6. Bending strength as a function of pore former content at different compaction pressures.

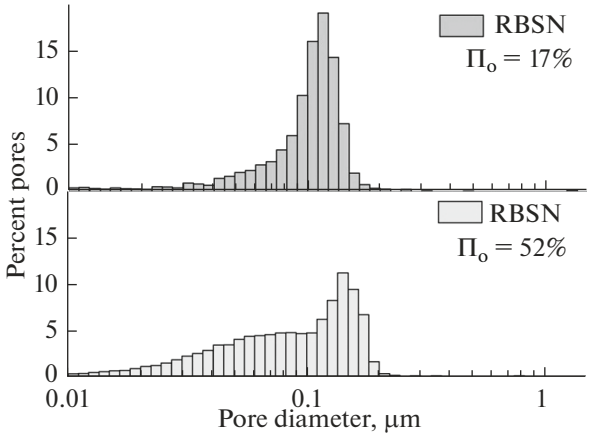

Fig. 7. Pore size distributions in ceramic samples (Hg porosimetry data).

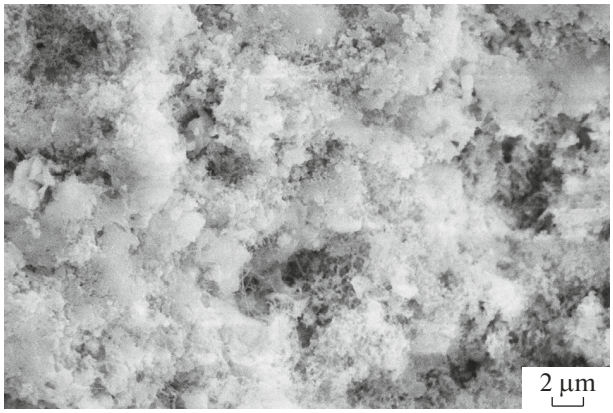

Fig. 8. SEM micrograph of a highly porous RBSN ceramic (Π_o = 52%).

size distribution: in the range from 0.01 to 0.1 μm. Therefore, the increase in porosity is mainly due to an increase in the number of small pores, which has an advantageous effect on the strength of the ceramic because, as reported by Park et al. [25], large pores markedly reduce the strength of the material.

The SEM image of a fracture surface of a ceramic sample in Fig. 8 demonstrates that the material has the form of a typical network of RBSN crystals, consisting predominantly of α-Si_3N_4, in good agreement with the X-ray diffraction data in Table 1.

It is worth noting that the ceramic samples obtained in this study contained no large pores, even though the presence of such pores was possible because the pore former used had an average particle size d_{av} ~ 9 μm. This apparent contradiction can be resolved in terms of the mechanism underlying RBSN synthesis [26], during which growing silicon nitride crystals (whiskers) fill cavities formed by the pore former. As a result, a continuous network of whiskers produces submicron porosity, which is detected by mercury porosimetry and SEM.

The dielectric permittivity of the ceramics decreases with increasing porosity. In particular, the ceramic samples with an open porosity of 52% have ε = 3.2, which is almost a factor of 2 lower than the dielectric permittivity of RBSN. Similar results were reported by Li et al. [12] and Zhou et al. [24]; that is, the ε values obtained in this study correspond to the expected level.

To assess thermophysical properties of the ceramics, we measured their heat capacity C_p and thermal diffusivity a and calculated their thermal conductivity λ. The 200 and 900°C LTECs of the highly porous ceramic samples with porosities of 42, 45, and 52% and their λ at 20 and 1000°C are presented in Table 3 in comparison with data for RBSN-based ceramics [4].

The thermal conductivity of the porous silicon nitride is considerably lower than that of RBSN [4]. The ceramic samples with a 52% porosity have λ = 1.27 W/(m K) at room temperature and 0.97 W/(m K) at 1100°C. The decrease in thermal conductivity is due to not only the decrease in porosity but also the high content of the α-phase (the thermal conductivity of α-Si_3N_4 single crystals is a factor of 2–2.5 lower than that of β-Si_3N_4 single crystals [9]) and the presence of about 11% Si_2N_2O inclusions (λ < 5 W/(m K) [5]). Moreover, according to elemental analysis data the pore former used in this study contained 8.6% amorphous SiO_2 (λ ~ 0.7–0.8 W/(m K) 4]), which was incorporated into the structure of the ceramics and, hence, further reduced their thermal conductivity.

Table 3. Effect of pore former content on the main properties of highly porous RBSN

Material	Weight percent of the pore former in the compacts	Π_o, %	$\alpha_{20-t} \times 10^7$, K^{-1}		λ, W/(m K)	
			200°C	900°C	20°C	1100°C
RBSN [4]	0	17	21 ± 3	32 ± 3	20	10
RBSN	25	42	19 ± 3	30 ± 3	2.71	2.15
	30	45	19 ± 3	30 ± 3	2.55	1.96
	40	52	18 ± 3	29 ± 3	1.27	0.96

CONCLUSIONS

We have proposed a process for the preparation of porous RBSN ceramics. It includes the addition of a pore former, uniaxial pressing, and reaction sintering.

The nitridation of porous green compacts has been shown to ensure the preparation of silicon nitride with a large percentage of the α-phase, which suggests that the nitridation reaction reaches near completion before the silicon begins to melt because all of the silicon particles are well accessible for nitrogen. This is expected to allow for a reduction in the maximum process temperature and duration.

Raising the compaction pressure increases the strength of the porous ceramics owing to the densification of the solid component. The samples prepared via pressing at 200 MPa have a bending strength of 48 MPa at a 50% porosity.

The proposed method has made it possible to considerably reduce the thermal conductivity and dielectric permittivity of RBSN, to $\lambda = 0.96$ W/(m K) at 1100°C and $\varepsilon = 3.2$ and $\tan\delta = 35 \times 10^{-4}$ at a frequency of 10 GHz, maintaining its strength at a level of ≥40 MPa. This opens up the possibility of using the material obtained in this study in heat-loaded elements of structures for aerospace applications.

REFERENCES

1. Andrievskii, R.A. and Spivak, I.I., *Nitrid kremniya i materialy na ego osnove* (Silicon Nitride and Related Materials), Moscow: Metallurgiya, 1984.
2. Ziegler, G., Heinrich, J., and Wotting, G., Relationships between processing, microstructure and properties of dense and reaction-bonded silicon nitride, *J. Mater. Sci.,* 1987, vol. 22, pp. 3041–3086.
3. Nair, R.U., Vandana, S., Sandhya, S., and Jha, R.M., Temperature-dependent electromagnetic performance predictions of a hypersonic streamlined radome, *Prog. Electromagn. Res.,* 2015, vol. 154, pp. 65–78.
4. Romashin, A.G., Gaidachuk, V.E., Karpov, Ya.S., and Rusin, M.Yu., *Radioprozrachnye obtekateli letatel'nykh apparatov. Proektirovanie, konstruktsionnye materialy, tekhnologiya proizvodstva, ispytaniya. Uchebnoe posobie* (Streamlined Radomes for Aircraft: Design Engineering, Structural Materials, Technological Aspects of Production, and Testing. A Learning Guide), Kharkiv: Nats. Aerokosm. Univ. "Kharkiv. Aviatsionnyi Institut," 2003, p. 239.
5. Zhou, Y., Hyuga, H., Kusano, D., Yoshizawa, Y., Ohji, T., and Hirao, K., Development of high-thermal-conductivity silicon nitride ceramics, *J. Asian Ceram. Soc.,* 2015, vol. 3, pp. 221–229. https://doi.org/10.1016/j.jascer.2015.03.003
6. Kitayama, M., Hirao, K., Toriyama, M., and Kanzaki, S., Thermal conductivity of β-Si_3N_4: effect of various microstructural factors, *J. Am. Ceram. Soc.,* 1999, vol. 82, no. 11, pp. 3105–3112.
7. Kaidash, O.N., Fesenko, I.P., and Kryl', Ya.A., Heat conductivity, physicomechanical properties and interrelations of them and structures of pressureless sintered composites produced of Si_3N_4–Al_2O_3–Y_2O_3(–ZrO_2) nanodispersed system, *J. Superhard Mater.,* 2014, vol. 36, no. 2, pp. 96–104.
8. Watari, K., Hirao, K., and Toriyama, M., Effect of grain size on the thermal conductivity of Si_3N_4, *J. Am. Ceram. Soc.,* 1999, vol. 82, no. 3, pp. 777–779.
9. Hirosaki, N., Ogata, S., Kocer, C., et al., Molecular dynamics calculation of the ideal thermal conductivity of single-crystal α- and β-Si_3N_4, *Phys. Rev. B: Condens. Matter Mater. Phys.,* 2002, vol. 65, no. 134 110. https://doi.org/10.1103/PhysRevB.65.134110
10. Antsiferov, V.N. and Gilev, V.G., Properties of porous silicon-nitride materials, *Ogneupory,* 1988, no. 7, pp. 20–23.
11. Kornienko, P.A., Naumenko, V.Ya., Chekhovich, V.A., et al., Strength and thermophysical properties of porous silicon nitride materials, *Sov. Powder Metall. Met. Ceram.,* 1984, vol. 23, no. 11, pp. 875–877.
12. Li, J.-Q., Fa, L., Zhu, D.-M., and Zhou, W.-C., Preparation and dielectric properties of porous silicon nitride ceramics, *Trans. Nonferrous Met. Soc. China,* 2006, vol. 16, pp. 487–489.
13. Jiang, G.-P., Yang, J.-F., and Gao, J.-Q., Porous silicon nitride ceramics prepared by extrusion using starch as binder, *J. Am. Ceram. Soc.,* 2008, vol. 91, no. 11, pp. 3510–3516. https://doi.org/10.1111/j.1551-2916.2008.02701.x
14. Fukasawa, T., Deng, Z.-Y., and Ando, M., Synthesis of porous silicon nitride with unidirectionally aligned channels using freeze-drying process, *J. Am. Ceram. Soc.,* 2002, vol. 85, no. 9, pp. 2151–2155. https://doi.org/10.1111/j.1151-2916.2002.tb00426.x
15. Gonzenbach, U.T., Studart, A.R., Tervoort, E., and Gauckler, L.J., Macroporous ceramics from particle-stabilized wet foams, *J. Am. Ceram. Soc.,* 2007, vol. 90, no. 1, pp. 16–22. https://doi.org/10.1111/j.1551-2916.2006.01328.x
16. Li, X., Wub, P., and Zhu, D., Effect of foaming pressure on the properties of porous Si_3N_4 ceramic fabricated by a technique combining foaming and pressureless sintering, *Scr. Mater.,* 2013, vol. 68, no. 11, pp. 877–880. https://doi.org/10.1016/j.scriptamat.2013.02.033
17. Yu, J., Yang, J., Li, H., Xi, X., and Huang, Y., Study on particle-stabilized Si_3N_4 ceramic foams, *Mater. Lett.,* 2011, vol. 65, no. 12, pp. 1801–1804. https://doi.org/10.1016/j.matlet.2011.03.082
18. Kandi, K.K. Thallapalli, N., et al., Development of silicon nitride-based ceramic radomes, *Int. J. Appl. Ceram. Technol.,* 2015, vol. 12, no. 5, pp. 909–920. https://doi.org/10.1111/ijac.12305
19. Li, B., Jiang, P., Yan, M.-W., Li, Y., Hou, X.-M., and Chen, J.-H., Characterization and properties of rapid fabrication of network porous Si_3N_4 ceramics, *J. Alloys Compd.,* 2017, vol. 709, pp. 717–723. https://doi.org/10.1016/j.jallcom.2017.03.223

20. Walton, J.D., *Proc. 2nd Int. Conf. on Electromagnetic Windows,* Paris, 1971, vol. 2, pp. 8–10.

21. Sillapasa, K., Danchaivijit, S., and Sujirote, K., Effects of silicon powder size on the processing of reaction-bonded silicon nitride, *J. Met., Mater. Miner.,* 2005, vol. 15, no. 2, pp. 97–102.

22. Kawai, C. and Yamakawa, A., Effect of porosity and microstructure on the strength of Si_3N_4: designed microstructure for high strength, high thermal shock resistance, and facile machining, *J. Am. Ceram. Soc.,* 1997, vol. 80, no. 10, pp. 2705–2708.

23. Danforth, S.C., Jennings, H.M., and Richman, M.H., The influence of microstructure on the strength of reaction bonded silicon nitride (RBSN), *Acta Metall.,* 1979, vol. 27, no. 1, pp. 123–130.

24. Zhou, J., Fan, J.-P., Sun, G.-L., Zhang, J.-Y., et al., Preparation and properties of porous silicon nitride ceramics with uniform spherical pores by improved pore-forming agent method, *J. Alloys Compd.,* 2015, vol. 632, pp. 655–660. https://doi.org/10.1016/j.jallcom.2015.01.305

25. Park, D.-S., Lee, M.-W., Kim, H.-D., Park, Y.-J., and Jung, Y.-G., Fabrication and properties of porous RBSN, *Key Eng. Mater.,* 2005, vol. 287, pp. 277–281. https://doi.org/10.4028/www.scientific.net/KEM.287.277

26. Moulson, A.J., Reaction-bonded silicon nitride: its formation and properties, *J. Mater. Sci.,* 1979, vol. 14, no. 5, pp. 1017–1051. https://doi.org/10.1007/BF00561287

Translated by O. Tsarev